PHYSICAL REVIEW D **81,** 104037 (2010)

Manifold corrections on spinning compact binaries

Shuang-Ying Zhong* and Xin Wu†

Nanchang University, Nanchang 330031, China

(Received 1 March 2010; published 18 May 2010)

This paper deals mainly with a discussion of three new manifold correction methods and three existing ones, which can numerically preserve or correct all integrals in the conservative post-Newtonian Hamiltonian formulation of spinning compact binaries. Two of them are listed here. One is a new momentum-position scaling scheme for complete consistency of both the total energy and the magnitude of the total angular momentum, and the other is the Nacozy's approach with least-squares correction of the four integrals including the total energy and the total angular momentum vector. The post-Newtonian contributions, the spin effects, and the classification of orbits play an important role in the effectiveness of these six manifold corrections. They are all nearly equivalent to correct the integrals at the level of the machine epsilon for the pure Kepler problem. Once the third-order post-Newtonian contributions are added to the pure orbital part, three of these corrections have only minor effects on controlling the errors of these integrals. When the spin effects are also included, the effectiveness of the Nacozy's approach becomes further weakened, and even gets useless for the chaotic case. In all cases tested, the new momentum-position scaling scheme always shows the optimal performance. It requires a little but not much expensive additional computational cost when the spin effects exist and several time-saving techniques are used. As an interesting case, the efficiency of the correction to chaotic eccentric orbits is generally better than one to quasicircular regular orbits. Besides this, the corrected fast Lyapunov indicators and Lyapunov exponents of chaotic eccentric orbits are large as compared with the uncorrected counterparts. The amplification is a true expression of the original dynamical behavior. With the aid of both the manifold correction added to a certain low-order integration algorithm as a fast and high-precision device and the fast Lyapunov indicators of two nearby trajectories, phase space scans for chaos in the spinning compact binary system are given.

DOI: 10.1103/PhysRevD.81.104037 PACS numbers: 02.70.−c, 04.25.Nx, 05.45.Pq, 45.10.−b

I. INTRODUCTION

Spinning compact binaries consisting of neutron stars or black holes, as a high nonlinear and nonintegrable relativistic two-body problem, are a rich source for potential chaos whose signature lies in sensitive dependence on initial conditions. Because the presence of chaos would affect future gravitational-wave detections, its investigation has received intense attention in recent years.

Whether two different post-Newtonian (PN) approximations to the black hole pair exhibit chaos is mainly considered in the literature. One is the PN Lagrangian formulation describing the orbital evolution of black hole pairs in harmonic coordinates [1–3], and the other relates to the PN Hamiltonian formulation determining the motion of two compact bodies in Arnowitt-Deser-Misner coordinates [4–6]. An earlier paper [7] confirmed with the method of fractal basin boundaries that the 2PN Lagrangian dynamics of a comparable-mass binary system having one spinning body (or two spins restricted to the leading order spin-orbit interaction) is chaotic. However, the method of finding parametric solutions indicates the absence of chaos in the corresponding 2PN Hamiltonian dynamics [8,9]. These facts show that the two formulations have different dynamical behaviors [10] although they are proved to be approximately equivalent [2,4]. When two objects spin and the spin effects include the spin-spin coupling as well as the leading order spin-orbit interaction, the 2PN Lagrangian dynamics was said to be chaotic [7,11,12]. The result was also supported by other references [13–15] in terms of different methods for identifying chaos, such as the frequency map analysis [13] and the invariant fast Lyapunov indicators of two nearby trajectories [14,15]. Here are some brief introductions to the history and the details of these methods for distinguishing between ordered and chaotic motion. The frequency analysis method of Laskar and his associates [16–18], as an improvement of the method of power spectrum [19–21], can detect chaos much faster from order than the method of Lyapunov exponents, and find the fundamental frequencies of the regular orbits. It is also suitable for a system with many degrees of freedom. Its main application lies in identifying order and chaos in the solar system dynamics [16]. Of course, the fast Lyapunov indicator method with the length of a tangent vector increasing in completely different time rates for ordered and chaotic orbits, introduced by Froeschlé *et al.* [22,23], is also a quicker method to find chaos. So is the smaller alignment index with the magnitude of the difference or the sum of two normalized

*zhongshuangying@ncu.edu.cn
†xwu@ncu.edu.cn

tangent vectors at the same orbit decreasing in completely different time rates for the two types of orbits, made by Skokos [24]. A comparison of the various methods can be found in the book entitled *Order and Chaos in Dynamical Astronomy* written by Contopoulos [25]. On the other hand, matched with this Lagrangian approach, the 2PN Hamiltonian dynamics admits the onset of chaos [26].

The above investigations of chaos in spinning compact binaries rely mainly on numerical integration algorithms, which are only referred to as conventional numerical integration schemes like Runge-Kutta–type integrators rather than symplectic integration algorithms [27–30]. Unfortunately, roundoff and truncation errors are not avoided at all during a process of numerical integration. Usually the small errors make the numerical solution dissatisfy the related integrals of motion, such as six conserved quantities involving the total energy, the total angular momentum vector, and the constant lengths of spins in the conservative 3PN Hamiltonian formulation for spinning compact binaries [5,6]. Especially for the instability of gravitational systems (e.g. the Kepler problem as the Newtonian limit of the formulation, and chaotic orbits) in the Lyapunov sense [31,32], such small errors will often become unbounded with time. In this case, the numerical solution will be far from the original hypersurface constrained by the integrals, i.e., its true solution. The stabilization of differential equations of Baumgarte [33] and the manifold correction of Nacozy [34] seem to be powerful tools for weakening or eliminating the instability influence on the numerical solution.

Baumgarte's method [33] relates to the use of modified and stabilized differential equations by adding some control terms (connected with known constraints) to the original unstable differential equations. In other words, its kernel is the application of stabilization to the set of equations by including the stabilizing terms. Its discussions and applications in satellite, asteroid, stellar, and planetary problems can be seen in Ref. [32]. Maybe because there is no universal rule for the choice of the optimal stabilizing parameter in this method, one pays much attention to the development and applicability of Nacozy's approach [34] in classical celestial mechanics. This approach applies the Lagrange multipliers least-squares corrections of a few integrals to obtain control terms, which are added to the numerical solution at the end of each time step so that the corrected numerical solution back onto the true manifolds of these integrals can be achieved. Moreover, it is named as the manifold correction [35], the projection method [36], or the post-stabilization method [37,38].

It is worth noting that the correction to both the total energy and the total angular momentum is not very efficient for an n-body simulation in the Solar System [36]. The reason was given in Refs. [39–41]. Instead, individual Kepler energies or angular momenta should be corrected. However, they are not constants of motion but vary slowly with time, so there seems to be an obstacle in the application of Nacozy's approach. Fortunately, more accurate reference values, obtained from the integral invariant relations [42] of these varying quantities in quasi-Keplerian motion, provide a good chance to implement this approach. Following this idea, the scaling method of Liu and Liao [43], the single scaling method of Fukushima [44], the velocity scaling method and the position scaling method of Ma *et al.* [45], as extensions to Nacozy's approach, can exactly satisfy the relation of the Keplerian energy for each planet or asteroid so as to improve the accuracy of the semimajor axis and the mean anomaly. Then, there are the dual scaling method [46] with correction of individual Keplerian energy and Laplace integral (equivalent to correcting the semimajor axis and the eccentricity), and the linear transformation method [47] with correction of individual Keplerian energy, Laplace integral and angular momentum vector (equivalent to improving all the orbital elements of each body). In fact, these belong to rigorous correction methods, which do strictly satisfy the relations of these slowly varying quasi-integrals. Almost equivalent to them in the correction effects, their corresponding approximate correction methods have recently been presented in Refs. [41,48–50].

In principle, the idea of a manifold correction can be used in PN celestial mechanics. Based on this point and our previous work [50] about the velocity scaling method with least-squares correction of some constraints, several new manifold correction methods will be designed for the conservative PN Hamiltonian formulation of spinning compact binaries. This becomes one of our main aims in the present paper. Another objective lies in evaluating how the PN contributions, the spin effects, and the classification of orbits exert influences on the effectiveness of the new correction schemes as well as some existing correction schemes involving Nacozy's approach. Above all, our ambition is to select the best of them as a reliable, fast, and high-precision device for some further insight into the dynamics of order and chaos in spinning compact binaries.

The remainder of this paper is constructed as follows. In Sec. II, all conserved quantities in the 3PN Hamiltonian formulation of spinning compact binaries are listed, and six new and old manifold correction methods for these invariants are given. Then numerical simulations and comparisons are arranged in Sec. III. As an application of the optimal manifold correction method, phase space scans for chaos in spinning compact binaries are shown in Sec. IV. Finally, Sec. V summarizes our conclusions. Geometric units $c = G = 1$ are used throughout the work.

II. PHYSICAL MODEL AND MANIFOLD CORRECTION SCHEMES

We introduce the Hamiltonian formulation of spinning compact binaries, its equations of motion, and its first integrals. Then several manifold correction schemes, in-

cluding the manifold correction of Nacozy [34] and the existing velocity (or momentum) scaling method with least-squares correction of some constraints [50], its extensions and its variants, are prepared for consistency of these integrals at every integration step.

A. The Hamiltonian formulation, evolution equations, and conserved quantities

For a relativistic system of spinning black hole pairs with masses m_1 and m_2 ($m_1 \leq m_2$), we take the total mass $M = m_1 + m_2$ and the reduced mass $\mu = m_1 m_2/M$, and also set $\eta = \mu/M = \beta/(1+\beta)^2$ with the mass ratio $\beta = m_1/m_2$. The dimensionless relative coordinate vector $\mathbf{r}$ is measured in terms of M, and its corresponding canonical momentum $\mathbf{p}$ in terms of μ. In this sense, the unit of time t has no choice but M. In the mean time we specify the scale r as the length of the vector $\mathbf{r}$, and let the unit vector $\mathbf{n}$ be $\mathbf{r}/r$. The dimensionless conservative 3PN Hamiltonian for describing center-of-mass motion of the relativistic two-body problem can be written as

$$H = H_O + H_S. \tag{1}$$

The first term H_O in the above equation denotes the pure orbital part including the Newtonian, 1PN, 2PN, and 3PN contributions, that is,

$$H_O = H_N + H_{1PN} + H_{2PN} + H_{3PN}. \tag{2}$$

Their detailed expressions read [5,6]

$$H_N = \frac{\mathbf{p}^2}{2} - \frac{1}{r}, \tag{3}$$

$$H_{1PN} = \frac{1}{8}(3\eta - 1)(\mathbf{p}^2)^2 - \frac{1}{2}[(3+\eta)\mathbf{p}^2 + \eta(\mathbf{n}\cdot\mathbf{p})^2]\frac{1}{r} + \frac{1}{2r^2}, \tag{4}$$

$$H_{2PN} = \frac{1}{16}(1 - 5\eta + 5\eta^2)(\mathbf{p}^2)^3 + \frac{1}{8}[(5 - 20\eta - 3\eta^2) \times (\mathbf{p}^2)^2 - 2\eta^2(\mathbf{n}\cdot\mathbf{p})^2\mathbf{p}^2 - 3\eta^2(\mathbf{n}\cdot\mathbf{p})^4]\frac{1}{r} + \frac{1}{2}[(5+8\eta)(\mathbf{p}^2) + 3\eta(\mathbf{n}\cdot\mathbf{p})^2]\frac{1}{r^2} - \frac{1}{4}(1+3\eta)\frac{1}{r^3}, \tag{5}$$

$$H_{3PN} = \frac{1}{128}(-5 + 35\eta - 70\eta^2 + 35\eta^3)(\mathbf{p}^2)^4 + \frac{1}{16}[(-7 + 42\eta - 53\eta^2 - 5\eta^3)(\mathbf{p}^2)^3 + (2 - 3\eta)\eta^2(\mathbf{n}\cdot\mathbf{p})^2(\mathbf{p}^2)^2 + 3(1-\eta)\eta^2(\mathbf{n}\cdot\mathbf{p})^4\mathbf{p}^2 - 5\eta^3(\mathbf{n}\cdot\mathbf{p})^6]\frac{1}{r} + \left[\frac{1}{16}(-27 + 136\eta + 109\eta^2)(\mathbf{p}^2)^2 + \frac{1}{16}(17 + 30\eta)\eta(\mathbf{n}\cdot\mathbf{p})^2\mathbf{p}^2 + \frac{1}{12}(5 + 43\eta)\eta(\mathbf{n}\cdot\mathbf{p})^4\right]\frac{1}{r^2} + \left\{\left[-\frac{25}{8} + \left(\frac{1}{64}\pi^2 - \frac{335}{48}\right)\eta - \frac{23}{8}\eta^2\right]\mathbf{p}^2 + \left(-\frac{85}{16} - \frac{3}{64}\pi^2 - \frac{7}{4}\eta\right)\eta(\mathbf{n}\cdot\mathbf{p})^2\right\}\frac{1}{r^3} + \left[\frac{1}{8} + \left(\frac{109}{12} - \frac{21}{32}\pi^2\right)\eta\right]\frac{1}{r^4}. \tag{6}$$

On the other hand, the second part H_S in Eq. (1), as spinning effects, is of the form [5,6]

$$H_S = H_{SO} + H_{SS}. \tag{7}$$

Here the spin-orbit coupling at 1.5PN order reads

$$H_{SO} = \frac{1}{r^3}\mathbf{L}\cdot\mathbf{S}_{\text{eff}} \tag{8}$$

with the Newtonian-looking angular momentum

$$\mathbf{L} = \mathbf{r}\times\mathbf{p} \tag{9}$$

(whose magnitude is $L = |\mathbf{L}|$) and

$$\mathbf{S}_{\text{eff}} = \left(2 + \frac{3}{2\beta}\right)\mathbf{S}_1 + \left(2 + \frac{3}{2}\beta\right)\mathbf{S}_2. \tag{10}$$

In addition, the spin-spin coupling at 2PN order is given by

$$H_{SS} = \frac{1}{2r^3}[3(\mathbf{S}_0\cdot\mathbf{n})^2 - \mathbf{S}_0^2] \tag{11}$$

with

$$\mathbf{S}_0 = (1 + 1/\beta)\mathbf{S}_1 + (1+\beta)\mathbf{S}_2. \tag{12}$$

Note that dimensionless spin variables are adopted and defined as

$$\mathbf{S}_i = \hat{\mathbf{S}}_i(\chi_i m_i^2/M^2) \qquad (i = 1, 2), \tag{13}$$

where $\hat{\mathbf{S}}_i$ represent unit spin vectors, and dimensionless parameters $\chi_i \in [0, 1]$. Through this treatment, the system (1) depends on no mass but the mass ratio.

The equations of motion about conjugate variables $(\mathbf{r}, \mathbf{p})$ satisfy the canonical forms

$$\frac{d\mathbf{r}}{dt} = \frac{\partial H}{\partial \mathbf{p}}, \qquad \frac{d\mathbf{p}}{dt} = -\frac{\partial H}{\partial \mathbf{r}}. \tag{14}$$

Meanwhile, the time evolutions of the two spins are [5,6]

$$\frac{d\hat{\mathbf{S}}_i}{dt} = \frac{\partial H}{\partial \mathbf{S}_i}\times\hat{\mathbf{S}}_i = \mathbf{\Omega}_i\times\hat{\mathbf{S}}_i, \tag{15}$$

where

$$\mathbf{\Omega}_1 = \left(2 + \frac{3}{2\beta}\right)\frac{\mathbf{L}}{r^3} + \frac{1}{\eta r^3}[3\mathbf{n}(\mathbf{S}_2 \cdot \mathbf{n}) - \mathbf{S}_2] + \frac{3}{r^3}(1 + 1/\beta)^2\mathbf{n}(\mathbf{S}_1 \cdot \mathbf{n}), \tag{16}$$

$$\mathbf{\Omega}_2 = \left(2 + \frac{3}{2}\beta\right)\frac{\mathbf{L}}{r^3} + \frac{1}{\eta r^3}[3\mathbf{n}(\mathbf{S}_1 \cdot \mathbf{n}) - \mathbf{S}_1] + \frac{3}{r^3}(1 + \beta)^2\mathbf{n}(\mathbf{S}_2 \cdot \mathbf{n}). \tag{17}$$

Obviously, the Hamiltonian (1) itself, called the total energy E, is a first integral of motion. Besides this, there are five integrals or conserved quantities, involving the total angular momentum [5,6]

$$\mathbf{J} = \mathbf{L} + \mathbf{S}_1 + \mathbf{S}_2 \tag{18}$$

(whose magnitude is $J = |\mathbf{J}|$) and the constant unit lengths of spins

$$\hat{S}_i = |\hat{\mathbf{S}}_i| = 1. \tag{19}$$

In total, six independent integrals exist in a 12-dimensional space made of variables $[\mathbf{r}, \mathbf{p}, \hat{\mathbf{S}}_1, \hat{\mathbf{S}}_2]$.

However, the existence of these six independent integrals does not imply the integrability of the system (1) owing to the use of these two noncanonical or nonconjugate spin variables whose time evolutions are Eq. (15) but unlike the canonical Hamiltonian equations (14). In fact, the 12-dimensional problem can be reduced to a 10-dimensional canonical form with symplectic structure [51], where four integrals including the total energy and the total angular momentum vector exist, but a fifth integral is absent. Because of this high nonlinearity and nonintegrability, the analytical solutions of the system cannot be obtained, but the numerical solutions easily can. Unfortunately, various errors in numerical integrations often cause the loss of these conserved quantities. That is to say, the errors may make the numerical solutions leave the 6-dimensional hypersurface determined by the integrals. In order to avoid it, we shall introduce some manifold correction schemes in which the numerical solutions are frequently readjusted to rigorously satisfy the identity relations (1), (18), and (19), or to approximately remain on the original integral hypersurface during the numerical integration.

B. Several manifold correction schemes

Assume that the system (1) has the total energy E_0 and the total angular momentum vector $\mathbf{J}_0$ (whose three components are $[J_{x0}, J_{y0}, J_{z0}]$, and whose magnitude is J_0) at the starting time. And suppose that H and $\mathbf{J}$ are, respectively, viewed as the energy and the angular momentum given by a true solution $[\mathbf{r}, \mathbf{p}, \hat{\mathbf{S}}_1, \hat{\mathbf{S}}_2]$ of the system at time t. As mentioned above, there are always $H = H(\mathbf{r}, \mathbf{p}, \hat{\mathbf{S}}_1, \hat{\mathbf{S}}_2) \equiv E_0$, $\mathbf{J} = \mathbf{J}(\mathbf{r}, \mathbf{P}, \hat{\mathbf{S}}_1, \hat{\mathbf{S}}_2) \equiv \mathbf{J}_0$, and $\hat{S}_i \equiv 1$. On the other hand, it is easy to obtain a numerical solution $[\mathbf{r}^*, \mathbf{p}^*, \hat{\mathbf{S}}_1^*, \hat{\mathbf{S}}_2^*]$ at the same time t by using a numerical scheme to integrate the evolution equations (14) and (15) for the system (1). The so-called computed (or integrated) solution corresponds to the computed energy $H^* = H(\mathbf{r}^*, \mathbf{p}^*, \hat{\mathbf{S}}_1^*, \hat{\mathbf{S}}_2^*)$, the computed angular momentum $\mathbf{J}^* = \mathbf{J}(\mathbf{r}^*, \mathbf{p}^*, \hat{\mathbf{S}}_1^*, \hat{\mathbf{S}}_2^*)$, the computed Newtonian angular momentum $\mathbf{L}^* = \mathbf{L}(\mathbf{r}^*, \mathbf{p}^*)$, and the computed spin lengths $\hat{S}_i^*$. Generally speaking, $H^* \neq E_0$, $\mathbf{J}^* \neq \mathbf{J}_0$, and $\hat{S}_i^* \neq 1$ because various errors in the computational procedure give rise to the computed solution different from the true one. In this sense, there is a simple way to find the relationship between the computed solution and its more accurate solution $[\bar{\mathbf{r}}, \bar{\mathbf{p}}, \hat{\bar{\mathbf{S}}}_1, \hat{\bar{\mathbf{S}}}_2]$ via spatial scale transformations to the computed solution, in which scale factors are determined by constraining the solution $[\bar{\mathbf{r}}, \bar{\mathbf{p}}, \hat{\bar{\mathbf{S}}}_1, \hat{\bar{\mathbf{S}}}_2]$ on the proper integral surfaces. Thus the more accurate solution, called the corrected solution, may become a good approximation to the true solution.

For corrections to the computed spin vectors $\hat{\mathbf{S}}_i^*$, a simple treatment is

$$\hat{\mathbf{S}}_i \approx \hat{\bar{\mathbf{S}}}_i = \hat{\mathbf{S}}_i^*/\hat{S}_i^*. \tag{20}$$

At once, the integrals (19) are exactly satisfied at each integration step. As to corrections to both the computed energy H^* and the computed angular momentum $\mathbf{J}^*$, several methods that adjust the coordinates or the momenta with the aid of scale transformations are presented as follows.

Method 1 (M1): A momentum scaling scheme with least-squares correction of four integrals.—This approach, which deals with both the use of only a scale transformation to the computed velocity (or momentum) vector and the determination of the scale factor based on the least-squares correction of the sum of the squares of errors of several integrals, was proposed in our previous work [50]. Now it is applied to suppress the accumulation of numerical errors in these integrals, Eqs. (1) and (18). The corrected momentum vector is expressed as

$$\mathbf{p} \approx \bar{\mathbf{p}} = \lambda \mathbf{p}^*, \tag{21}$$

where the scale factor λ is given by the minimizing error function

$$\Phi_1(\lambda) = w_1[H(\mathbf{r}^*, \bar{\mathbf{p}}, \hat{\bar{\mathbf{S}}}_1, \hat{\bar{\mathbf{S}}}_2) - E_0]^2 + w_2\{[J_x(\mathbf{r}^*, \bar{\mathbf{p}}, \hat{\bar{\mathbf{S}}}_1, \hat{\bar{\mathbf{S}}}_2) - J_{x0}]^2 + [J_y(\mathbf{r}^*, \bar{\mathbf{p}}, \hat{\bar{\mathbf{S}}}_1, \hat{\bar{\mathbf{S}}}_2) - J_{y0}]^2 + [J_z(\mathbf{r}^*, \bar{\mathbf{p}}, \hat{\bar{\mathbf{S}}}_1, \hat{\bar{\mathbf{S}}}_2) - J_{z0}]^2\}, \tag{22}$$

equivalently, its vanishing derivative

$$\Phi_1'(\lambda) = 0. \tag{23}$$

Note that w_1 and w_2 are two positive weight coefficients. In this case, λ can be solved from Eq. (23) in terms of an analytical method or a numerical method such as Newton's iterative method. Hereafter, the scaling correction scheme (21) is referred to as method 1 (M1).

Two points about this technique are worth emphasizing. It is clear from Eq. (21) that only the accuracy of the integrated momentum would be improved rather than that of the integrated position coordinates from a process of one integration step. However, the latter should also be raised during entire numerical integrations, as claimed in Refs. [41,45]. On the other hand, it is shown in Eq. (22) that the method may have a certain effectiveness of correction to any one of the four integrals by Eqs. (1) and (18), but does not completely.

Method 2 (M2): A momentum scaling scheme with least-squares correction of the total energy and the magnitude of the total angular momentum.—This technique still adopts the scale change (21) but the scale factor λ is derived from the least-squares correction of the total energy and the magnitude of the total angular momentum, that is, λ satisfies the relation

$$\Phi_2'(\lambda) = 0, \tag{24}$$

where

$$\Phi_2(\lambda) = w_1[H(\mathbf{r}^*, \bar{\mathbf{p}}, \hat{\bar{\mathbf{S}}}_1, \hat{\bar{\mathbf{S}}}_2) - E_0]^2 + w_2\{[J(\mathbf{r}^*, \bar{\mathbf{p}}, \hat{\bar{\mathbf{S}}}_1, \hat{\bar{\mathbf{S}}}_2) - J_0]^2\}. \tag{25}$$

Method 3 (M3): A momentum-position scaling scheme with least-squares correction of four integrals.—It is similar to M1 but uses two distinct scale factors (α and β) to, respectively, adjust the integrated momentum and the integrated position in the expressions

$$\mathbf{p} \approx \bar{\mathbf{p}} = \alpha \mathbf{p}^*, \qquad \mathbf{r} \approx \bar{\mathbf{r}} = \beta \mathbf{r}^*. \tag{26}$$

As in M1, the two scale factors are worked out by solving the equations

$$\frac{\partial \Phi_3}{\partial \alpha} = 0, \qquad \frac{\partial \Phi_3}{\partial \beta} = 0 \tag{27}$$

with the auxiliary quantity

$$\Phi_3(\alpha, \beta) = w_1[H(\bar{\mathbf{r}}, \bar{\mathbf{p}}, \hat{\bar{\mathbf{S}}}_1, \hat{\bar{\mathbf{S}}}_2) - E_0]^2 + w_2\{[J_x(\bar{\mathbf{r}}, \bar{\mathbf{p}}, \hat{\bar{\mathbf{S}}}_1, \hat{\bar{\mathbf{S}}}_2) - J_{x0}]^2 + [J_y(\bar{\mathbf{r}}, \bar{\mathbf{p}}, \hat{\bar{\mathbf{S}}}_1, \hat{\bar{\mathbf{S}}}_2) - J_{y0}]^2 + [J_z(\bar{\mathbf{r}}, \bar{\mathbf{p}}, \hat{\bar{\mathbf{S}}}_1, \hat{\bar{\mathbf{S}}}_2) - J_{z0}]^2\}. \tag{28}$$

Method 4 (M4): A momentum-position scaling scheme for complete consistency of both the total energy and the magnitude of the total angular momentum.—This is a combination of M2 and M3. That is to say, the method continues to use Eqs. (26) and (27) in which Φ_3 gives place to

$$\Phi_4(\alpha, \beta) = w_1[H(\bar{\mathbf{r}}, \bar{\mathbf{p}}, \hat{\bar{\mathbf{S}}}_1, \hat{\bar{\mathbf{S}}}_2) - E_0]^2 + w_2\{[J(\bar{\mathbf{r}}, \bar{\mathbf{p}}, \hat{\bar{\mathbf{S}}}_1, \hat{\bar{\mathbf{S}}}_2) - J_0]^2\}. \tag{29}$$

In this case, the two integrals are always preserved rigorously at each integration step, i.e.,

$$H(\bar{\mathbf{r}}, \bar{\mathbf{p}}, \hat{\bar{\mathbf{S}}}_1, \hat{\bar{\mathbf{S}}}_2) = E_0 \tag{30}$$

and

$$|\alpha\beta \mathbf{L}^* + \bar{\mathbf{S}}_1 + \bar{\mathbf{S}}_2| = J_0. \tag{31}$$

Substituting β [given by Eq. (31)] into Eq. (30), we can easily obtain the scaling factor α, too.

Method 5 (M5): A momentum-position scaling scheme with exact correction of the total energy and with least-squares correction of three components of the total angular momentum.—Here Eq. (30) is still considered, but Eq. (31) is replaced with

$$\frac{d}{d\beta}\Phi_5(\alpha, \beta) = 0, \tag{32}$$

where

$$\Phi_5(\alpha, \beta) = [J_x(\bar{\mathbf{r}}, \bar{\mathbf{p}}, \hat{\bar{\mathbf{S}}}_1, \hat{\bar{\mathbf{S}}}_2) - J_{x0}]^2 + [J_y(\bar{\mathbf{r}}, \bar{\mathbf{p}}, \hat{\bar{\mathbf{S}}}_1, \hat{\bar{\mathbf{S}}}_2) - J_{y0}]^2 + [J_z(\bar{\mathbf{r}}, \bar{\mathbf{p}}, \hat{\bar{\mathbf{S}}}_1, \hat{\bar{\mathbf{S}}}_2) - J_{z0}]^2, \tag{33}$$

and α is a function of β, determined by Eq. (30).

Method 6 (M6): Nacozy's approach.—Of course, the manifold correction scheme of Nacozy [34], which employs Lagrange multipliers to bring the corrected solution to fall on the true integral hypersurface along the shortest path, can be applied to stabilize the four integrals (1) and (18). Some details of its implementation are illustrated here. The integrated solution about the position and the momentum is marked as $\boldsymbol{X}^* = (x^*, y^*, z^*, p_x^*, p_y^*, p_z^*)^T$, where the T superscript denotes transpose. The error function vector is defined as $\boldsymbol{Y} = (H^* - E_0, J_x^* - J_{x0}, J_y^* - J_{y0}, J_z^* - J_{z0})^T$. The corrected solution is

$$\boldsymbol{X} \approx \bar{\boldsymbol{X}} = \boldsymbol{X}^* + \boldsymbol{\Delta X}^*, \tag{34}$$

where the correction vector added to the numerical solution is of the type

$$\boldsymbol{\Delta}\, \boldsymbol{X}^* = -\boldsymbol{W}^{-1}\boldsymbol{Z}^T(\boldsymbol{Z}\boldsymbol{W}^{-1}\boldsymbol{Z}^T)^{-1}\boldsymbol{Y}. \tag{35}$$

In the above equation, $\boldsymbol{W}$ is a 6×6 weighting matrix with rank 6, and $\boldsymbol{Z}$ stands for a 4×6 matrix (having rank 4) associated with partial derivatives of the integrals, namely,

TABLE I. Basic characteristics of several manifold correction methods. Here we suppose that a jth-order integrator with a time step of τ works in a double-precision environment, the order of 10^{-16}. J denotes the magnitude of the total angular momentum.

Correction method	M1	M2	M3	M4	M5	M6
Approach character	Approximate	Approximate	Approximate	Rigorous	Approximate	Approximate
Corrected variables	Momentum	Momentum	Momentum position	Momentum position	Momentum position	Momentum position
Energy accuracy	Unknown	Unknown	Unknown	10^{-16}	10^{-16}	$\mathcal{O}(\tau^{2(j+1)})$
Accuracy of J	Unknown	Unknown	Unknown	10^{-16}	Unknown	$\mathcal{O}(\tau^{2(j+1)})$
Literature	Ref. [50]	Ref. [50]	This work	This work	This work	Ref. [34]

$$\boldsymbol{Z} = \begin{bmatrix} \frac{\partial H}{\partial x} & \frac{\partial H}{\partial y} & \frac{\partial H}{\partial z} & \frac{\partial H}{\partial p_x} & \frac{\partial H}{\partial p_y} & \frac{\partial H}{\partial p_z} \\ \frac{\partial J_x}{\partial x} & \frac{\partial J_x}{\partial y} & \frac{\partial J_x}{\partial z} & \frac{\partial J_x}{\partial p_x} & \frac{\partial J_x}{\partial p_y} & \frac{\partial J_x}{\partial p_z} \\ \frac{\partial J_y}{\partial x} & \frac{\partial J_y}{\partial y} & \frac{\partial J_y}{\partial z} & \frac{\partial J_y}{\partial p_x} & \frac{\partial J_y}{\partial p_y} & \frac{\partial J_y}{\partial p_z} \\ \frac{\partial J_z}{\partial x} & \frac{\partial J_z}{\partial y} & \frac{\partial J_z}{\partial z} & \frac{\partial J_z}{\partial p_x} & \frac{\partial J_z}{\partial p_y} & \frac{\partial J_z}{\partial p_z} \end{bmatrix}_{(\boldsymbol{X}^*, \hat{\mathbf{S}}_1, \hat{\mathbf{S}}_2)}. \quad (36)$$

Each corrected integral contains a second-order accuracy of its uncorrected counterpart.

It should be pointed out that the six correction methods mentioned above are all originated from the idea of least-squares corrections, but have explicit differences in the performance of improving the accuracy of these integrals and the correction path of forcing the integrated solution back to the original integral hypersurface. The number of the corrected integrals is always more than that of the scale factors used in any one of the four methods M1, M2, M3, and M5. As a result, each of the integrals (except the energy integral in M5) has neither a complete correction nor a least-squares correction. Note that the least-squares correction is only applied to the sum of the squares of the errors of these integrals. However, M4, as a particular case that the number of the requested scale factors is just equal to one of the integrals of the total energy and the magnitude of the total angular momentum, can exactly keep the two integrals in numerical integrations. In addition, M6, unlike each of the four methods M1, M2, M3, and M5, gives the least-squares correction to individual integral. On the other hand, the correction direction is not normal to the hypersurface for each of the five methods M1–M5, but it is for M6. Table I lists some basic characteristics of these correction methods. Detailed numerical simulations will also be necessary to give further insight into the correction effectiveness of each method.

III. NUMERICAL COMPARISONS

The above manifold correction methods are used to control numerical errors of the related integrals according to three cases: the Newtonian two-body problem, the pure orbital part to the 3PN order, and the 3PN formulation having two spins.

A. The Newtonian two-body problem

A pure Kepler two-body problem (3), as the Newtonian limit of the system (1), holds the energy integral (3) and the angular momentum integrals (9). The corrections to these integrals are equivalent to ones to the orbital elements such as the semimajor axis, the inclination, and the longitude of the ascending node. In order to suppress the growth of integration errors in these elements, the rotation combined with the single scaling method was proposed in Ref. [52]. Since the rotation and the single scaling method are used independently, the energy integral and the angular momentum are not simultaneously corrected. Here we consider the applicability of the above manifold corrections. For the simplified case, the scale factors of M4 and M5 can be given explicitly. For M4 we have

$$\begin{aligned} \alpha &= [L^* + \sqrt{L^{*2} + 2E_0 L_0^2 r^{*2}\mathbf{p}^{*2}}]/(L_0 r^* \mathbf{p}^{*2}), \\ \beta &= L_0/(\alpha L^*). \end{aligned} \quad (37)$$

Additionally, the two scale factors in M5 are easily achieved by

$$\begin{aligned} \alpha &= [L^{*2} + \sqrt{L^{*2} + 2E_0 r^{*2}\mathbf{p}^{*2}(\mathbf{L}_0 \cdot \mathbf{L}^*)^2}]/[r^* \mathbf{p}^{*2}(\mathbf{L}_0 \cdot \mathbf{L}^*)], \\ \beta &= (\mathbf{L}_0 \cdot \mathbf{L}^*)/(\alpha L^{*2}). \end{aligned} \quad (38)$$

However, the determination of the scale factors for the three methods M1, M2, and M3 has to rely on the Newtonian method in which the iterative precision is desired to arrive at the order of 10^{-15}.

According to the suggestion of Ref. [50], we still take the weight coefficients $w_1 = 100$ and $w_2 = 1$. And let the weighting matrix $\boldsymbol{W}$ be a unit matrix. Now a fifth-order Runge-Kutta integrator (RK5) with a fixed time step of 0.2, as an uncorrected integrator, is used to integrate a quasi-circular (or small eccentricity) orbit with initial conditions of $(\mathbf{r}, \mathbf{p}) = (20, 0, 0, 0, 0.2461, 0)$. In fact, the orbit corresponds to its eccentricity $e = 0.1847$. As shown in Fig. 1 that draws numerical errors of both the energy and the length of the angular momentum varying with time for RK5 and its correction methods M1–M6, all these corrections compared with the uncorrected scheme RK5 have almost the same effect in drastically controlling the errors of the two integrals, even reaching the machine precision, the order of 10^{-16}. The result is also suitable for the pure orbital part to 1PN or 2PN order. Thus it can be concluded that the six correction methods are nearly effective in improving the quality of integration for the three cases of

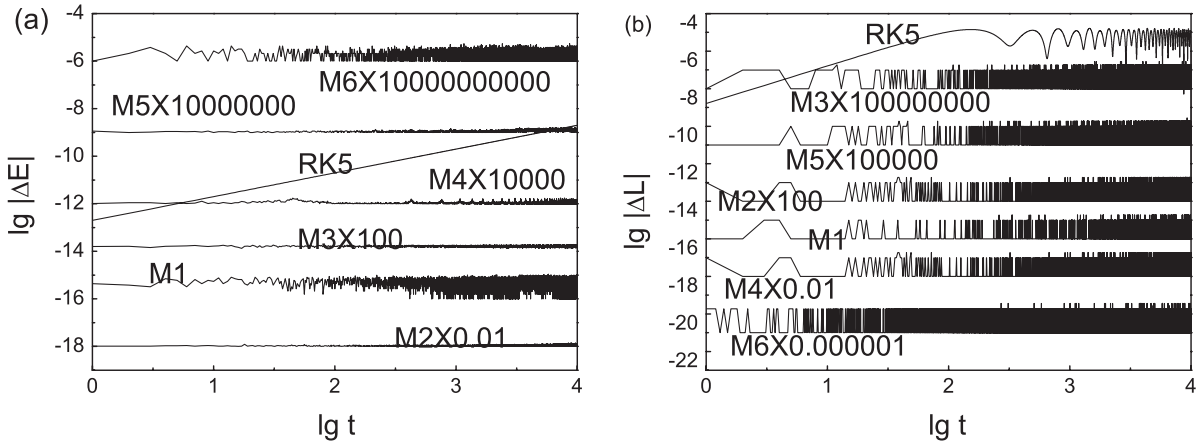

FIG. 1. Errors of the total energy (a) and the magnitude of the angular momentum (b) for RK5 and its correction schemes applied to the Kepler problem. As two examples to illustrate the related symbols, M2 $\times$ 0.01 denotes the plotted errors decreased by 100 times compared with the real ones for M2, while M3 $\times$ 100 indicates the plotted errors enlarged by 100 times.

the Newtonian problem, the 1PN and 2PN approximations. What about their performance for the pure orbital part to 3PN order? The following demonstration will answer it.

B. The 3PN nonspinning formulation

The pure orbital 3PN formulation (2) belongs to a typical perturbed Kepler problem that has the energy integral (2) and the angular momentum integrals (9). The existence of these integrals implies the integrability or the nonchaoticity of this canonical system. It is necessary to apply the Newtonian method to solve the scale factors of the five methods M1–M5. The above orbit is still used in this formulation with the mass ratio $\beta = 1/3$. Although there are the 1PN, 2PN, and 3PN contributions, the orbit provided by RK5 in Fig. 2(a) like its corresponding Keplerian orbit is always restricted to the x-y plane because the constant angular momentum vector is perpendicular to the plane at any time. As is expected, the corrected orbit from any correction scheme in Fig. 2(b) remains the same as the uncorrected one in Fig. 2(a). In fact they are both completely different if the integration lasts too long. An uncorrected regular orbit can become spurious chaos for a long time of numerical integration, but its corrected one cannot. See Fig. 5 of Ref. [45] or Fig. 1 of Ref. [50] for more details.

However, there are great differences in suppressing the errors of these integrals among the correction methods. Figures 2(b) and 2(c) display that the three methods M1, M2, and M3 have slighter corrections to either the energy or the angular momentum (except for M3) but do not bring more dramatic ones than the uncorrected scheme, RK5. On the contrary, M4, M5, and M6 play an important role in significantly reducing the errors of these conserved quantities down to the level of the machine epsilon. This illustrates clearly that the PN terms have a great effect on these correction methods. Next we want to know whether the validity depends on the spin effects.

C. The 3PN formulation with two spins

In order to further understand the effectiveness of various correction methods mentioned above, we are interested in the application of these methods to small eccentric orbits, higher eccentric orbits, and chaotic orbits in the comparable-mass compact binary system (1), where the 1.5PN order and 2PN order spin effects as well as the 1PN, 2PN, and 3PN pure orbital contributions are simultaneously added to the Newtonian problem (3).

1. A small eccentric regular orbit

The dynamical parameters we used are $\beta = 1/3$ and $\chi_1 = \chi_2 = 0.75$. The initial conditions of the chosen orbit (labeled as orbit 1) are the same as those in Fig. 2, and the starting unit spin configurations $\hat{\mathbf{S}}_1 = (\sin\theta_1, 0, \cos\theta_1)$ and $\hat{\mathbf{S}}_2 = (\sin\theta_2, 0, \cos\theta_2)$ with initial spin angles $\theta_1 = \pi/6$ and $\theta_2 = \pi/4$ are chosen. As stated above, the corresponding Keplerian orbit is small eccentric or quasicircular.

By means of RK5, we get a three-dimensional view of the orbit in Fig. 3(a) that indicates the occurrence of the precession motion. This tells us the dependence of the precession of the orbital plane on the spin contributions. Through the treatment of the manifold correction method M4, the obtained three-dimensional view in Fig. 3(b) is very similar to the one in Fig. 3(a), but some difference between them exists indeed from the projection onto the x-p_x plane. The tours without any correction in Fig. 3(c) have a small width formed by a series of discretized points, while the one with correction in Fig. 3(d) becomes extremely thinner. A similar result can also be found from the projection onto the x-y plane, colored gray in panels (a) and (b).

As far as the classification of the orbit in Fig. 3 is concerned, power spectra with a discrete frequency distribution of the time series of the x component in Fig. 4(a) turn out to show the regularity of the orbit. This fact is also

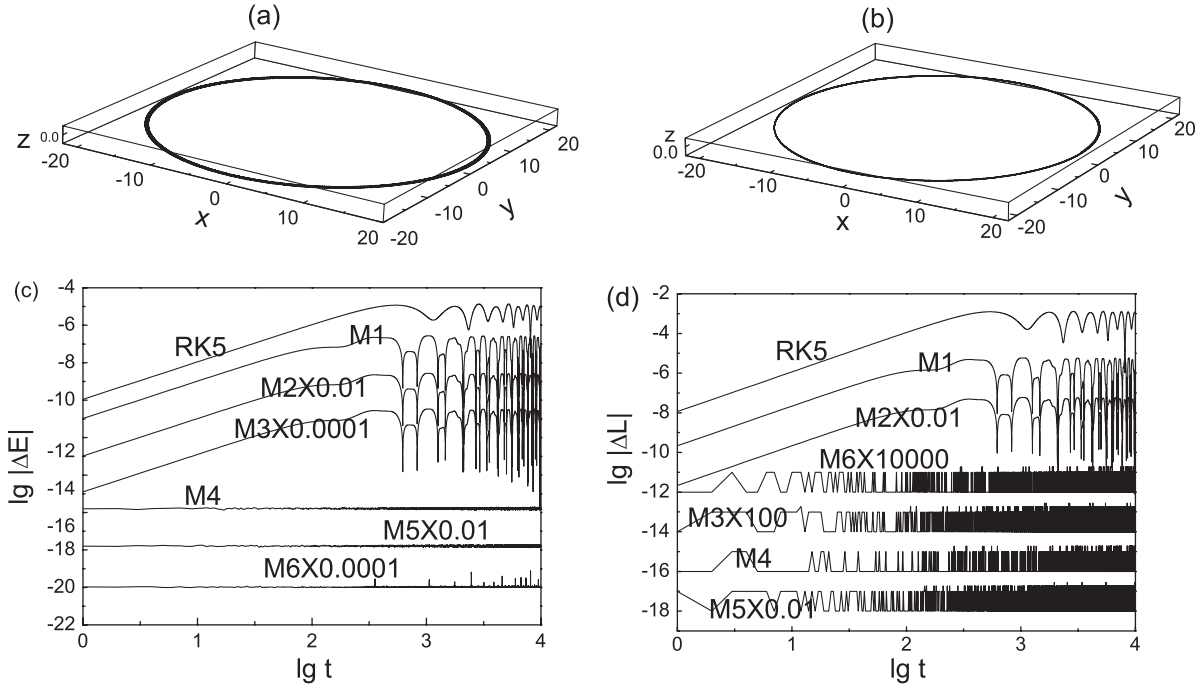

FIG. 2. A 3PN orbit with initial conditions of $(\mathbf{r}, \mathbf{p}) = (20, 0, 0, 0, 0.2461, 0)$ and the mass ratio $\beta = 1/3$ without any spin and its errors in the total energy and the angular momentum. (a) relates to the uncorrected orbit, and (b) to the corrected one with M4.

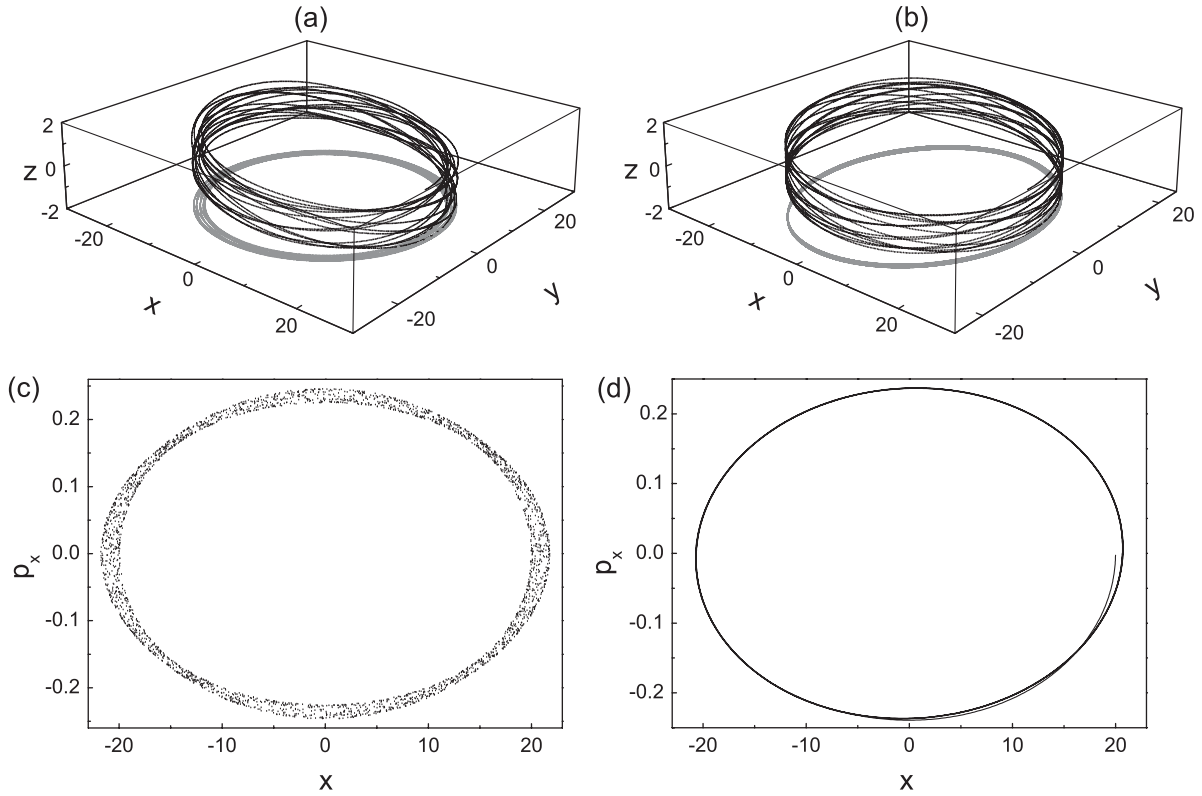

FIG. 3. A quasicircular orbit with initial conditions and mass ratio the same as those of Fig. 2 in the case of two starting unit spin configurations $\hat{\mathbf{S}}_1 = (\sin\frac{\pi}{6}, 0, \cos\frac{\pi}{6})$ and $\hat{\mathbf{S}}_2 = (\sin\frac{\pi}{4}, 0, \cos\frac{\pi}{4})$ and spin parameters $\chi_1 = \chi_2 = 0.75$. (a) is the three-dimensional view yielded by the uncorrected scheme RK5, where the bottom code-colored gray denotes the projection of the orbit onto the x-y plane. (b) relates to the correction of (a) with M4. Both (c) and (d) are the uncorrected and corrected projections of the orbit onto the x-p_x plane, respectively. Obviously, the corrected tours become thinner than the uncorrected ones.

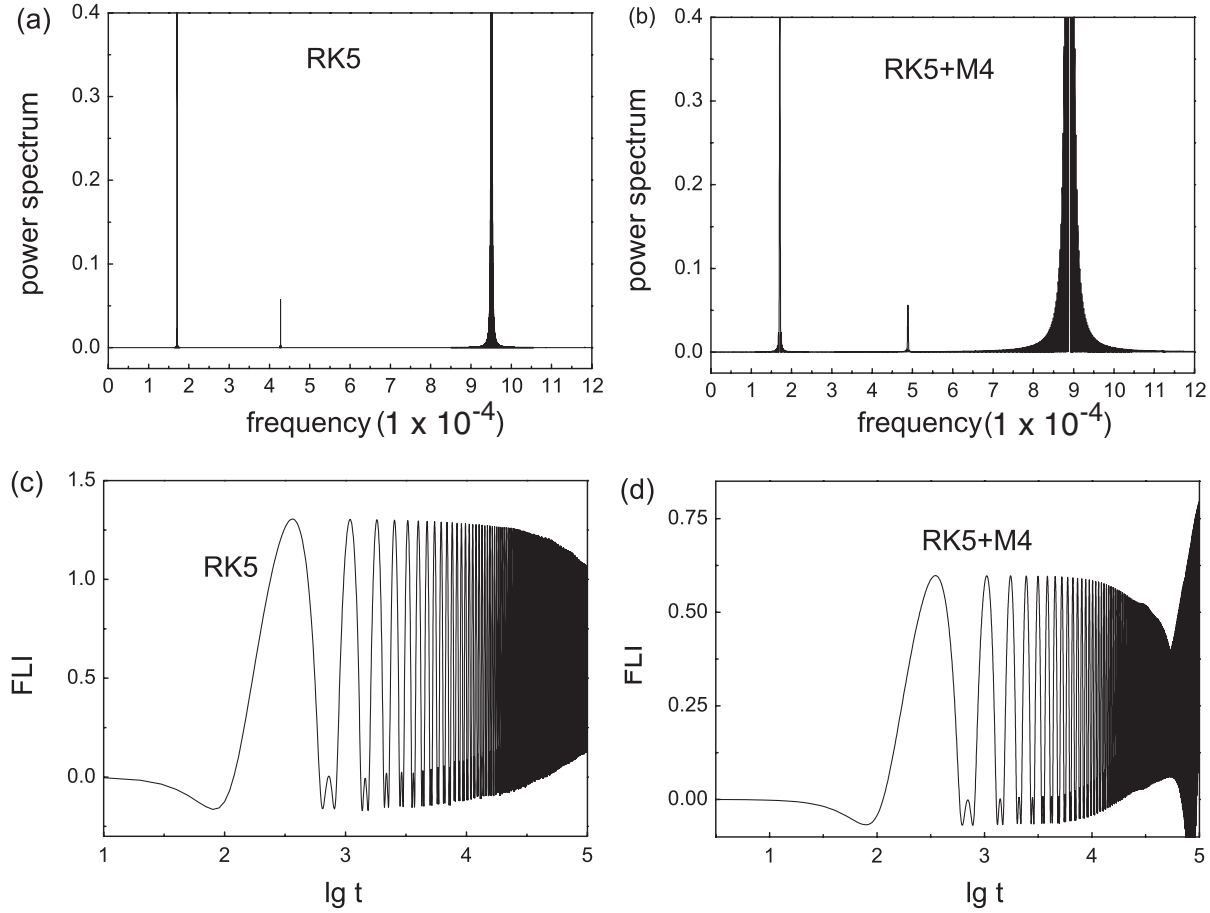

FIG. 4. Comparison of the power spectra between the uncorrected (a) and corrected (b) cases for the orbit in Fig. 3. The bottom panels are the same as the top ones but to the fast Lyapunov indicators (FLIs).

supported by the fast Lyapunov indicator (FLI) that measures the power-law divergence of initially close trajectories with time in Fig. 4(c). Notice that both the corrected power spectra and FLIs on the right-hand side of Fig. 4 and the uncorrected ones on the left-hand side are nearly compatible. As a point to illustrate, the FLI we adopted is based on the one with two-nearby trajectories and its algorithm proposed in Ref. [53]. This indicator is defined as

$$\mathrm{FLI}\,(t) = \lg[d(t)/d_0], \tag{39}$$

where d_0 and $d(t)$ represent the separations of the two trajectories at times 0 and t, respectively. Although it is not a coordinate-invariant indicator mentioned in [54,55], the identification of chaos is unambiguous in the adopted space-time coordinates. It is said to be a more sensitive tool to detect chaos from order than the method of Lyapunov exponents [14]. It has been applicable to the study of the dynamics of some complicated systems [15,56,57]. Because of this advantage, it is used frequently in later discussions of this paper.

On the other hand, Fig. 5 indicates that the spin part (3) does greatly affect the effectiveness of these correction methods. The corrected errors in the integrals including the total energy and the total angular momentum for the methods M1, M2, and M3 are slightly less than or almost the same as the uncorrected errors for RK5. Roughly speaking, the corrections become basically useless. In particular, Nacozy's approach M6 does not provide very idealized corrections. Meanwhile it is easy to see that M4 is the best method in the control of the errors. M4 makes the errors of the integrals almost equal or close to the limit of the computer capability. These results should be reasonable since M4 itself satisfies strictly the two integrals from the theoretical point of view (note that M5 also gives an exact correction to the energy), but the rest does approximately. In addition, it is worth emphasizing that the implementation of M4 or M5 becomes more difficult or needs a rather larger additional computational expense in the spinning case than it does in the nonspinning case. Here are several time-saving techniques during the correction procedure. First, the scaling factor β appearing in all denominators should be killed before the iterative method is used to solve the two scaling factors. Second, the iteration should end and the obtained values of the scaling factors should be outputted when the number of iterations

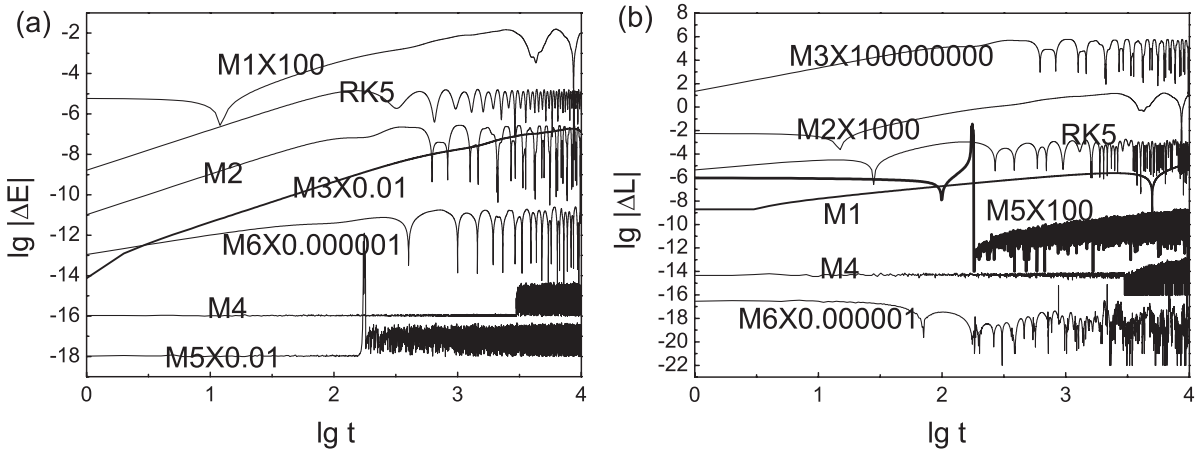

FIG. 5. Errors in the total energy and the total angular momentum for the orbit of Fig. 3.

is added up to 1500 even if the requested iterative precision with respect to the scaling factors is not satisfied. As an illustration, the energy accurate to the order of 10^{-16} and the angular momentum to the order of 10^{-14} within some time span for M4 show that the scaling factors have achieved the requested iterative precision, while slightly poorer accuracies of the energy and the angular momentum at the approach of the final integration time indicate that the scaling factors have not yet. Third, the iteration should also stop when the number of iterations does not reach 1500 but the scaling factor β is as small as the order of 10^{-12}, so extremely smaller denominators can be avoided to appear in the equations of motion.

Considering the spin effects making the correction methods M1, M2, and M3 have a poor performance in controlling these integral errors and noting M5 inferior to M4, we focus on a comparison between M4 and M6 in later numerical checks.

2. A higher eccentric regular orbit

Now we choose an orbit (labeled as orbit 2) that holds initial conditions $(\mathbf{r}, \mathbf{p}) = (20, 0, 0, 0, 0.265, 0)$, initial spin angles $\theta_1 = \theta_2 = \pi/4$, and dynamical parameters $\beta = 1$ and $\chi_1 = \chi_2 = 0.75$. Its corresponding Keplerian orbit has larger eccentricity $e = 0.4045$.

Seen from a three-dimensional view of the orbit in Fig. 6(a), the precession motion yields still. Although the three-dimensional orbit and its projection onto the x-y plane in Fig. 6(b) are obtained from the uncorrected integrator RK5, they are very similar when the correction M4 is added. In addition, they seem to indicate that the orbit is typically ordered. The methods of power spectra and FLIs (whose diagrams are not plotted) also support this point.

It is easy to observe that the corrected errors of the energy and the angular momentum given by M4 and M6 for the larger eccentric orbit in Fig. 7 are similar to those for the quasicircular orbit in Fig. 5. That is to say, Nacozy's

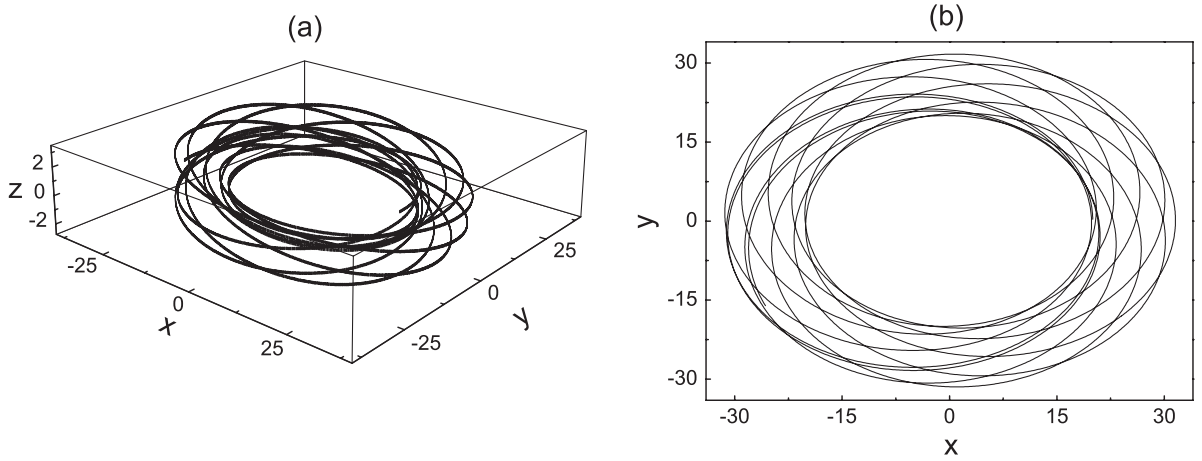

FIG. 6. An eccentric orbit with initial conditions $(\mathbf{r}, \mathbf{p}) = (20, 0, 0, 0, 0.265, 0)$, parameters $\beta = 1$ and $\chi_1 = \chi_2 = 0.75$, and initial spin angles $\theta_1 = \theta_2 = \pi/4$. (a) and (b) represent a three-dimensional view of the orbit and its projection onto the x-y plane, respectively.

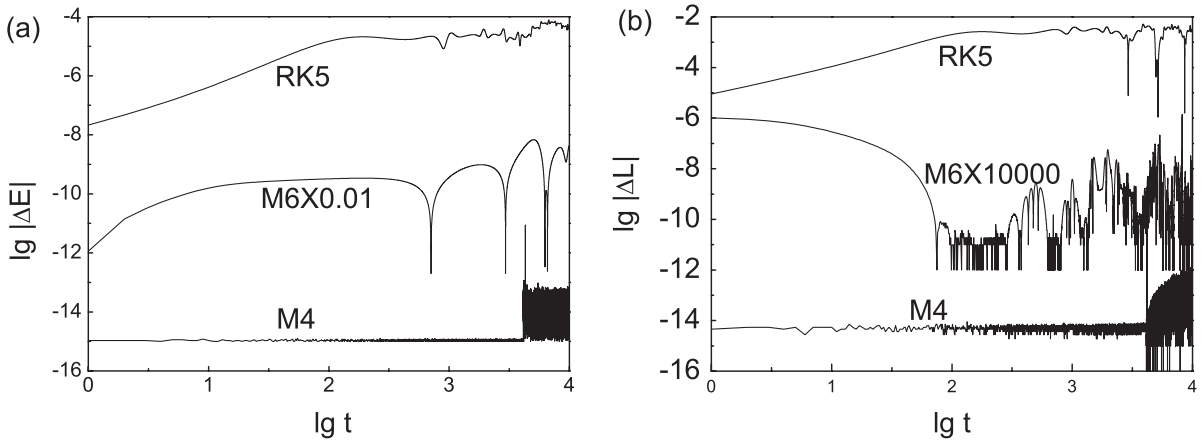

FIG. 7. Similar to Fig. 5, but for the eccentric orbit in Fig. 6.

approach M6 has smaller corrections to either the energy or the angular momentum than the uncorrected scheme RK5, while the method M4 provides more dramatic ones. Still there is the problem that these scaling factors for M4 cannot reach the desired iterative precision under the limited number of iterations when integration time is close to the end.

Besides the cases of smaller and larger eccentricities, how chaotic eccentric orbits affect the correction effectiveness of both M4 and M6 is worth paying attention to. See the next numerical tests for more information.

3. A chaotic eccentric orbit

The spinning compact binary system is full of the high nonlinearity, so it becomes a rich source of hiding potential chaos. Chaos can occur in the conservative Hamiltonian dynamics of spinning compact binaries with the spin effects at 2PN order and the pure orbital part to 2PN or 3PN order. This fact was confirmed in Ref. [26]. Without a doubt, chaos must increase the degree of the numerically artificial dissipation. What about these corrections for this case?

Let us consider the case of two maximal spin magnitudes, namely, spin parameters $\chi_1 = \chi_2 = 1$, and take the mass ratio $\beta = 1$. Initial conditions of an orbit marked as orbit 3 are $(\mathbf{r}, \mathbf{p}) = (5.658, 0, 0, 0, 0.764\,580\,5, 0)$, corresponding to the Newtonian orbital eccentricity $e = 0.3076$. Meanwhile initial unit spin vectors are chosen as $\hat{\mathbf{S}}_1 = (0.130\,36, 0.262\,852, -0.955\,989)$ and $\hat{\mathbf{S}}_2 = (0.118\,966, -0.134\,59, -0.983\,734)$. When RK5 is still used as a numerical tool, the three-dimensional orbit embedded in Euclidian space is drawn in Fig. 8(a). The orbit looks to exhibit a highly stochastic motion. So does the projection onto the x-y plane in Fig. 8(b). As a point to illustrate, the three-dimensional view and its projection onto the plane agree closely with those when the correction

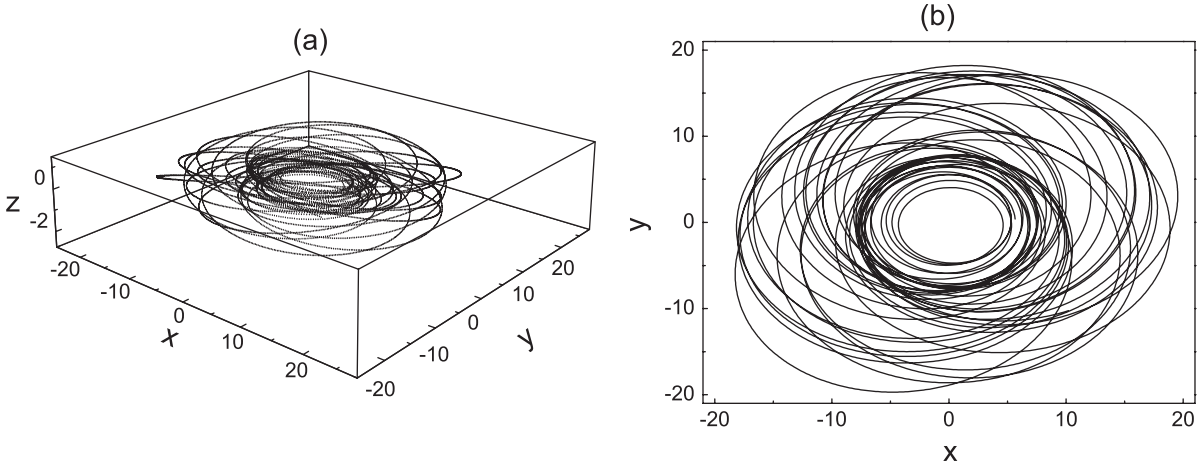

FIG. 8. A chaotic eccentric orbit of two maximally spinning compact binaries with initial conditions $(\mathbf{r}, \mathbf{p}) = (5.658, 0, 0, 0, 0.764\,580\,5, 0)$, dynamical parameters $\chi_1 = \chi_2 = 1$ and $\beta = 1$, and initial unit spin vectors $\hat{\mathbf{S}}_1 = (0.130\,36, 0.262\,852, -0.955\,989)$ and $\hat{\mathbf{S}}_2 = (0.118\,966, -0.134\,59, -0.983\,734)$. Both the three-dimensional view (a) and its projection (b) onto the x-y plane are given by RK5.

M4 or M6 is added. However, this does not mean that there is not any difference in the corrections of the total energy and the magnitude of the total angular momentum between M4 and M6. As we expect, M4 can achieve the ideal corrections to either the total energy or the magnitude of the total angular momentum, but M6 has no correction effect. Their details are provided in Fig. 9.

To our surprise, M4 is so powerful to correct these errors that the scaling factors can be given in the desired iterative precision before the limited number of iterations at every integration step. The case is in disagreement with those of the above-mentioned quasicircular regular orbit 1 and eccentric regular orbit 2 because of the basic dynamical character of orbit 3. Both the power spectra with a continuous frequency distribution in Fig. 10(a) and the FLIs having the exponential-law divergence of initially close trajectories with time in Fig. 10(c) indicate the chaoticity of orbit 3. Certainly, chaos with exponential sensitivity on small variations of initial conditions results in a rapid increase of various numerical errors and Lyapunov's orbital instability, but this just gives a good chance for the application of a manifold correction scheme. It is mainly based on the task of the correction scheme, which suppresses the fast accumulation of these errors. In other words, the faster the artificial dissipation gets, the more necessary the use of the correction is, and the more apparent the effect of the correction becomes. Therefore, the scaling factors become quicker to obtain for the chaotic case than they do for the above regular orbits.

Now we want to know how the manifold correction scheme M4 exerts influences to the power spectra, the FLIs, and the Lyapunov exponents for the chaotic orbit. It is clearly shown in Figs. 10(a) and 10(b) that the corrected power spectra on the right-hand side coincide basically with the uncorrected ones on the left-hand side. In addition, the corrected FLIs and the uncorrected ones are almost the same before an integration time span of about 10 000, as shown in Fig. 10(c). Since then, a separation between them has begun to produce, and the value of the corrected FLI has always been over that of the uncorrected FLI at the same time. This seems to tell us that the manifold correction leads to a chaotic amplification effect, or some increase in the strength of chaos. Similarly, the manifold correction also has an effect on the amplification of a Lyapunov exponent. The Lyapunov exponent in Fig. 10(d) is referred to as the slope of the line $\ln[d(t)/d_0]$ vs t. This is called the least-squares fit method for the computation of Lyapunov exponents. In principle, the calculation of Lyapunov exponents should have used the limit method by obtaining the stabilizing limit values about the natural logarithm of the divergence rate of nearby trajectoriesversus time averages, namely,

$$\gamma = \lim_{t\to\infty} \frac{1}{t} \ln \frac{d(t)}{d_0}. \tag{40}$$

However, usually the fit method is easier to identify the regularity or the chaoticity than the limit method during a short time [14]. Because of this, the fit method is used to compute Lyapunov exponents in some references [12,26,58]. A practical problem is whether the amplification of both the FLIs and the Lyapunov exponents given by the manifold correction has an overestimation or physical significance. As a check, we employ higher-precision integrators such as an 8th–9th order Runge-Kutta-Fehlberg algorithm of variable time step and the 12th order Adams-Cowell method to recalculate the FLIs and the Lyapunov exponents. Consequently, it is found that these results obtained from the higher-order integrators are nearly consistent with those given by RK5 plus the manifold correction M4. This means that the amplification caused by the manifold correction is not spurious. Here is an interpretation for it. When the manifold correction is used, the preservation of these 6 conserved quantities is always rigorous during the numerical integration so that a numerical solution is strictly restricted on a hypersurface of 6 dimensions. However, the artificial dissipation makes the

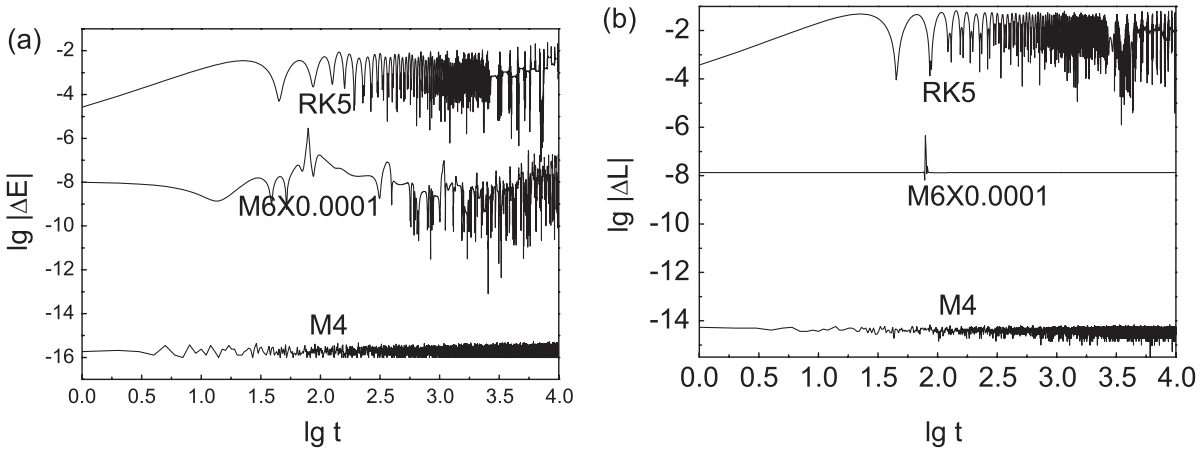

FIG. 9. Similar to Fig. 7, but for the chaotic orbit of Fig. 8.

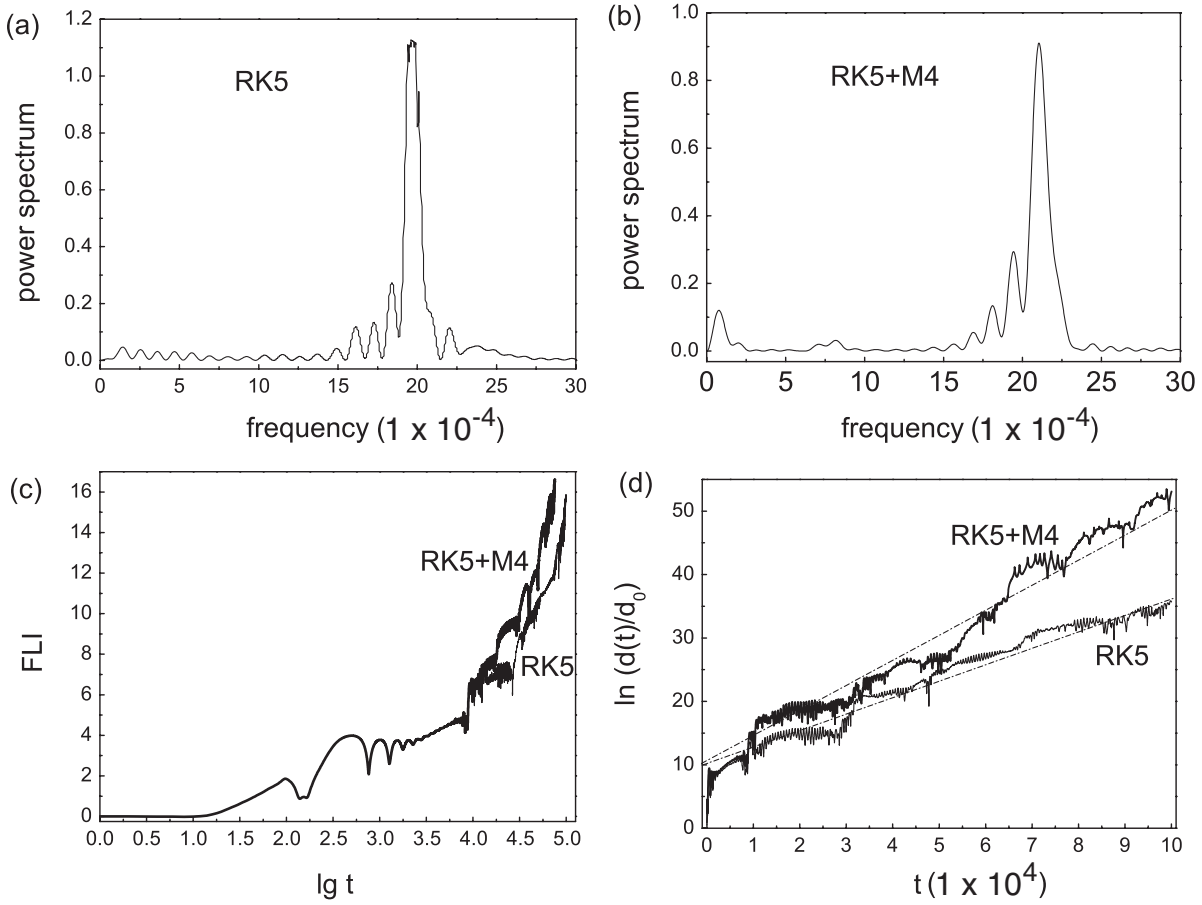

FIG. 10. (a) and (b) correspond to the uncorrected power spectra and the corrected ones for the chaotic orbit of Fig. 8. (c) shows comparisons between the uncorrected and corrected FLIs, and (d) shows those between the uncorrected and corrected Lyapunov exponents as the slopes of the lines $\ln[d(t)/d_0]$ vs t. Clearly, the corrected FLIs and slope are larger than the uncorrected ones after $t = 10\,000$.

numerical orbit relatively free and relaxed for the case without any correction, equivalently, run beyond the 6-dimensional hypersurface. Thus the strength of chaos becomes weaker in some degree under the existence of the artificial dissipation. In fact, the chaos damped by another dissipation, called the gravitational dissipation at the 2.5PN order radiation reaction term, was uncovered in Ref. [12]. Although the two kinds of dissipations are originated from completely distinct mechanisms, they should play a similar role in damping chaos. In brief, these facts and analysis show that the manifold correction does keep some dynamical properties even for the chaotic case. Inversely, the chaotic case makes the manifold correction apparently efficient, and leads to the fast convergence of the scaling factors, as compared with the regular case.

By comparison with these results obtained in the above numerical tests, a summary is concluded here. The effectiveness of the above-mentioned six manifold correction methods depends closely on the twofold, different approximations to the same physical system and classification of orbits. Above all, both the spin effects and the chaotic feature of orbits have an important effect on corrections to either the total energy or the magnitude of the total angular momentum. Some details are described in the following. For the Kepler problem as case 1, the six manifold correction methods work almost equivalently in keeping the errors of the total energy and the magnitude of the total angular momentum at the level of the machine epsilon. Nevertheless, the PN contributions for the 3PN nonspinning formulation (case 2) make each of the manifold corrections M1, M2, and M3 improve the quality of these integrals only somewhat. Especially for case 3 (the 3PN formulation with two spinning objects), the existence of the spin effects greatly affects the validity of these corrections. Any one of the manifold corrections M1, M2, and M3 gives only minor correction effects, or roughly speaking, becomes invalid for orbit 1, the quasicircular regular orbit. The correction M5 is relatively superior to M6, but inferior to M4. It is particularly interesting to see that M4 demonstrates the best performance of corrections for orbit 3, the chaotic eccentric orbit. This time, M6 becomes almost useless. As a clear expression of the

TABLE II. Errors ΔE of the total energy and errors ΔJ of the magnitude of the total angular momentum for RK5 and its manifold correction methods. Cases 1, 2, and 3 correspond to the Kepler problem, the 3PN nonspinning formulation, and the 3PN formulation having two spinning objects, respectively. Orbits 1, 2, and 3 are in sequence referred to as the quasicircular regular orbit in Fig. 3, the higher eccentric regular orbit of Fig. 6, and the chaotic eccentric orbit in Fig. 8.

Method		RK5	M1	M2	M3	M4	M5	M6
Case 1	ΔE	10^{-8}	10^{-16}	10^{-16}	10^{-16}	10^{-16}	10^{-16}	10^{-16}
	ΔJ	10^{-5}	10^{-15}	10^{-15}	10^{-15}	10^{-15}	10^{-15}	10^{-15}
Case 2	ΔE	10^{-6}	10^{-7}	10^{-7}	10^{-8}	10^{-16}	10^{-16}	10^{-16}
	ΔJ	10^{-4}	10^{-7}	10^{-7}	10^{-15}	10^{-15}	10^{-15}	10^{-15}
Case 3	ΔE	10^{-6}	10^{-4}	10^{-7}	10^{-5}	10^{-15}	10^{-14}	10^{-8}
Orbit 1	ΔJ	10^{-4}	10^{-6}	10^{-5}	10^{-4}	10^{-14}	10^{-10}	10^{-14}
Case 3	ΔE	10^{-5}	⋯	⋯	⋯	10^{-15}	⋯	10^{-10}
Orbit 2	ΔJ	10^{-4}	⋯	⋯	⋯	10^{-14}	⋯	10^{-11}
Case 3	ΔE	10^{-4}	⋯	⋯	⋯	10^{-15}	⋯	10^{-4}
Orbit 3	ΔJ	10^{-3}	⋯	⋯	⋯	10^{-14}	⋯	10^{-4}

performance of these corrections in all cases tested, Table II shows a comparison of the average errors of the total energy and the magnitude of the total angular momentum during the final integration time. On the other hand, these corrections should also have some apparent differences at the cost of additional computations. These corrections have a negligibly small increase in additional computational labor for cases 1 and 2. So they except the corrections M4 and M5 when the spin contributions are added. However, the spin effects cause M4 and M5 to need much additional computational time because more iterations are required to solve the scaling factors. For the sake of time savings, the number of iterations is limited even if the desired iterative precision is not reached. Through this treatment, the correction M4 requires a little but not much expensive additional computational cost. Note that the use of the correction becomes more expensive for orbit 1 than the one for orbit 3 because the convergence of the scaling factors is slower for the former. Detailed CPU times about these corrections are displayed in Table III.

In conclusion, of all the above-mentioned manifold correction methods, M4 is thought of as the optimal correction method. It can drastically reduce the integration errors especially for the chaotic case. Even if a low-order integrator (e.g. RK5) combined with the manifold correction M4 is adopted, the obtained qualitative results on the dynamical information should be reliable. Because of this, the correction M4 with the FLIs will be worth recommending to give phase space scans for chaos so that the dynamics of spinning compact binaries can be further investigated.

TABLE III. CPU times(s) of all the cases tested in Table II.

Method	RK5	M1	M2	M3	M4	M5	M6
Case 1	9	10	10	10	10	10	10
Case 2	9	10	10	10	11	11	11
Orbit 1	10	12	12	12	40	30	15
Orbit 2	10	⋯	⋯	⋯	30	⋯	14
Orbit 3	10	⋯	⋯	⋯	27	⋯	14

IV. PHASE SPACE SCANS FOR CHAOS

A sensitivity to chaos depends on the variation of any of the degrees of freedom as well as the mass ratio of the two spinning compact objects. Numerical investigations are impossible to cover all variations finding chaos. In this instance our scan searching for the presence of chaos is limited only to the variation of two initial spin directions with the aid of both M4 added to RK5 and the FLIs.

Let us begin to trace a transition to chaos as one of the two spin angles is varied initially. Some details of the implementation are as follows. We fix the dynamical parameters of the mass ratio $\beta = 1/4$ and the spin parameters $\chi_1 = \chi_2 = 1$, initial conditions $(\mathbf{r}, \mathbf{p}) = (5.658, 0, 0, 0, 0.764\,580\,5, 0)$, and the first starting spin angle $\theta_1 = \pi/2$, whereas the second starting spin angle θ_2 ranges from 0 to π with a span of $\Delta\theta_2 = 0.01$. In total, 314 orbits are integrated numerically. Consequently, the value of the FLI for each orbit is obtained after an integration time span of 10^5. All the FLIs of Fig. 11(a) show an abrupt change in the dynamics from order to chaos. The transition occurs when θ_2 exceeds approximately 2.78, corresponding to FLIs larger than 5.8 as the threshold between order and chaos. If the mass ratio $\beta = 1/4$ is replaced only with $\beta = 1$, the transition to chaos shifts slightly from $\theta_2 = 2.78$ to $\theta_2 = 2.38$, as shown in Fig. 11(b). It should be emphasized that the chaotic orbits and the strength of chaos are mainly located near $\theta_2 = \pi$ for the two cases. This coincides basically with the result of [26] that chaos appears in the $(10 + 10)M_\odot$ configuration when initial spin vectors are nearly antialigned with the Newtonian-looking orbital angular momentum $\mathbf{L}$. It can be seen much clearly from the case of varying the two initial spin angles. Figure 12(a) is a scan for chaos by calculating the FLIs of 314×314 orbits on the (θ_1, θ_2) plane. The black domains relate to chaotic initial spin angles with FLIs larger than 5.8, and the gray areas stand for regular initial spin angles with FLIs less than 5.8. Obviously, there is a strong chaotic belt in a neighborhood of a point (π, π), but there is no chaos at all in some regions far away from this point, especially including one region around the point $(\pi/2, \pi/2)$ and another domain near the point (0, 0). That is to say, chaos completely disappears when the initial spins are both perpendicular to or aligned with the orbital angular momentum. Saying this in another way, the spin coupling effects are weak in these cases, while strong around the point (π, π). Is it suitable for other fixed dy-

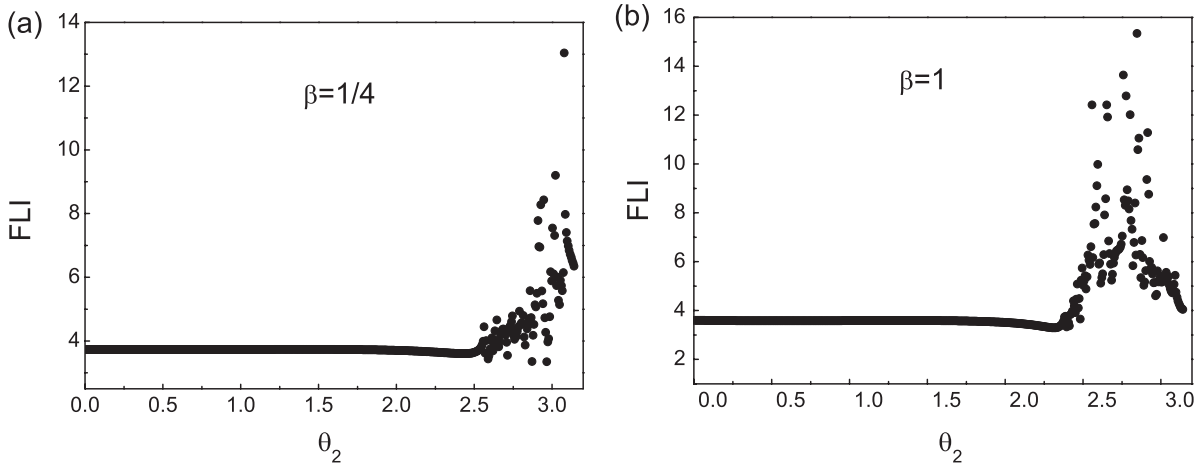

FIG. 11. FLI as a function of initial spin angle θ_2 with fixed initial states $r = 5.658$, $p_y = 0.764\,580\,5$ and $\theta_1 = \pi/2$, and spin parameters $\chi_1 = \chi_2 = 1$.

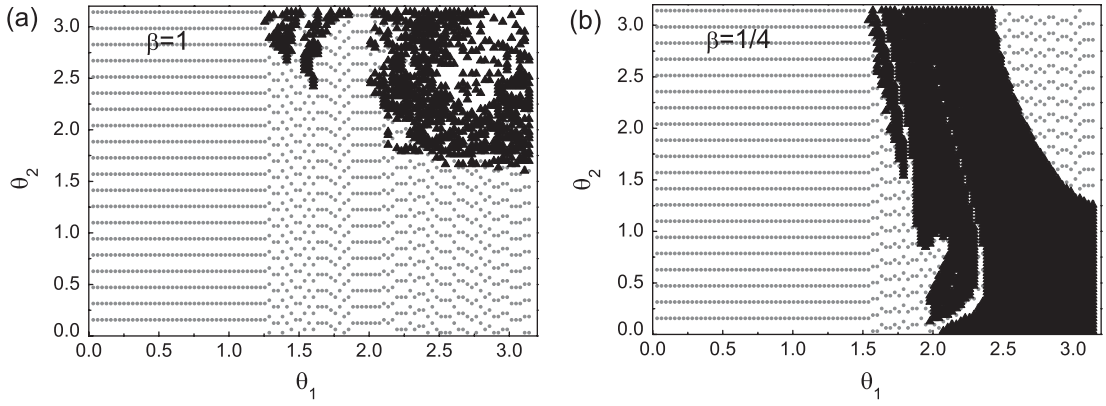

FIG. 12. Similar to Fig. 11, but scans of a group of initial points on the θ_1-θ_2 plane for chaos. Black areas with FLIs > 5.8 indicate chaos, and gray areas with FLIs ≤ 5.8 show order.

namical parameters, initial positions, and momenta? No, as an answer, is shown in Fig. 12(b) that uses only $\beta = 1/4$ instead of $\beta = 1$. Unlike Fig. 12(a), this panel describes that chaos is absent near the point (π, π), but present for initial spin angles $\theta_1 \in (1.5, \pi]$ and huge numbers of initial spin angles $\theta_2 \in [0, \pi]$. The difference is because the onset of chaos depends on not only a single physical parameter or initial condition, but also a complicated combination of all parameters and initial conditions. In this sense, the dependence of chaos on a certain parameter or initial condition should alter when other fixed dynamical parameters or initial conditions are chosen. This is just a further check of the work [15], where the dynamics of the 2PN Lagrangian formulation for spinning compact binaries was resurveyed. In addition, it is worth noting that Fig. 12(b) apparently contains the fractal meaning.

V. SUMMARY

The conservative PN Hamiltonian formulation for spinning compact binaries holds six integrals of motion, the total energy, the total angular momentum vector, and the constant lengths of the two spin vectors. A scale transformation to each spin can exactly preserve the constant magnitude of the spin at every integration step. For the sake of the numerical preservation or correction to the rest integrals, several new and existing manifold correction methods are considered. They include the method M1 as an existing momentum scaling scheme [50] with least-squares correction of the four integrals consisting of the total energy and the total angular momentum vector, the method M2 being an existing momentum scaling scheme [50] with least-squares correction of the total energy and the magnitude of the total angular momentum, the method M3 belonging to a new momentum-position scaling scheme with least-squares correction of the four integrals, the method M4 corresponding to a new momentum-position scaling scheme for complete consistency of both the total energy and the magnitude of the total angular momentum, the method M5 on a new momentum-position scaling scheme with exact correction of the total energy and with least-squares correction of three components of

the total angular momentum, and the method M6 from Nacozy's approach to the four integrals [34]. Although these corrections are all based on the idea of least-squares corrections, there are explicit differences that each of the four methods M1, M2, M3, and M5 gives only the least-squares correction to the sum of the squares of the errors of these integrals (except the energy integral for M5), while M6 does one to an individual integral, and M4 can rigorously maintain the two integrals of the total energy and the magnitude of the total angular momentum during numerical integrations. In addition, the correction of M6 except any of the leading five corrections pulls the numerical solution back to the real integral hypersurface along the shortest path.

The PN contributions, the spin effects, and the classification of orbits are regarded as three important sources for affecting the effectiveness of these manifold correction methods. Any or all of these corrections can remain as the accuracy of the total energy and the magnitude of the total angular momentum at the level of the machine epsilon for the pure Kepler case. However, the manifold corrections M1, M2, and M3 have only minor effects on controlling the errors of these conserved quantities when the pure orbital part to 3PN contributions is considered. In particular, the spin effects make the manifold corrections M1, M2, and M3 useless. Even Nacozy's approach M6 can hardly work well for chaotic eccentric orbits. In all cases tested, M4 is confirmed to be the best manifold correction in drastically enhancing the quality of orbit integrations. On the other hand, these three sources lead to different computational efficiency of the above-mentioned corrections. The additional computational cost of each of the six correction needs is negligibly small when the spin effects are turned off. It is still valid to those except M4 and M5 for the spin effects included. In this case, the limited number of iterations for solving the two scaling factors, as one of the time-saving techniques, is necessarily applicable to M4 or M5. Thus, the correction M4 requires a little but not much expensive additional computational cost. A point to note is that chaotic eccentric orbits become easier in the application of this correction than quasicircular regular orbits.

Inversely, the correction M4 can exert some influences to an integrated orbit as compared with the case without correction. These influences may refer to a 3-dimensional view of the orbit, its projection onto a certain plane, the power spectra, the FLIs, and the Lyapunov exponents. When integration time of a regular orbit is not long, they should not be apparently different between the corrected case and the uncorrected one. However, for the chaotic case the manifold correction gives rise to the amplification of both the FLIs and the Lyapunov exponents compared with the uncorrected counterparts. The amplification is not spurious. This shows sufficiently that the manifold correction can maintain some dynamical features, and be viewed as a powerful tool to get rid of Lyapunov's orbital instability and to suppresses the fast growth of the errors.

According to the above-mentioned main points, we generally recommend the addition of the manifold correction M4 to a low-order integration algorithm as a fast and high-precision device with which to simulate the orbital evolution of spinning compact binaries. Using this treatment and the FLIs, we give the phase space scan for chaos and further check the result of [15] to see that there is no universal rule on the relationship between the transition to chaos and single varying physical parameter or initial condition when other fixed dynamical parameters and initial conditions have different choices.

ACKNOWLEDGMENTS

This research is supported by the Natural Science Foundation of China under Contract No. 10873007. It is also supported by the Science Foundation of Jiangxi Education Bureau (GJJ09072), and the Program for Innovative Research Team of Nanchang University.

[1] L. E. Kidder, Phys. Rev. D **52**, 821 (1995).
[2] V. C. de Andrade, L. Blanchet, and G. Faye, Classical Quantum Gravity **18**, 753 (2001).
[3] G. Faye, L. Blanchet, and A. Buonanno, Phys. Rev. D **74**, 104033 (2006).
[4] T. Damour, P. Jaranowski, and G. Schäfer, Phys. Rev. D **63**, 044021 (2001).
[5] T. Damour, Phys. Rev. D **64**, 124013 (2001).
[6] A. Buonanno, Y. Chen, and T. Damour, Phys. Rev. D **74**, 104005 (2006).
[7] J. Levin, Phys. Rev. Lett. **84**, 3515 (2000).
[8] C. Königsdörffer and A. Gopakumar, Phys. Rev. D **71**, 024039 (2005).
[9] A. Gopakumar and C. Königsdörffer, Phys. Rev. D **72**, 121501(R) (2005).
[10] J. Levin, Phys. Rev. D **74**, 124027 (2006).
[11] J. Levin, Phys. Rev. D **67**, 044013 (2003).
[12] N. J. Cornish and J. Levin, Phys. Rev. D **68**, 024004 (2003).
[13] Y. Xie and T. Y. Huang, Chin. J. Astron. Astrophys. **6**, 705 (2006).
[14] X. Wu and Y. Xie, Phys. Rev. D **76**, 124004 (2007).
[15] X. Wu and Y. Xie, Phys. Rev. D **77**, 103012 (2008).
[16] J. Laskar, Icarus **88**, 266 (1990).
[17] J. Laskar, C. Froeschlé, and A. Celletti, Physica (Amsterdam) **56D**, 253 (1992).

[18] J. Laskar, Physica (Amsterdam) **67D**, 257 (1993).
[19] D. W. Noid, M. Koszykowski, and R. A. Marcus, J. Chem. Phys. **67**, 404 (1977).
[20] J. Binney and D. Spergel, Astrophys. J. **252**, 308 (1982).
[21] J. Binney and D. Spergel, Mon. Not. R. Astron. Soc. **206**, 159 (1984).
[22] C. Froeschlé, E. Lega, and R. Gonczi, Celest. Mech. Dyn. Astron. **67**, 41 (1997).
[23] C. Froeschlé and E. Lega, Celest. Mech. Dyn. Astron. **78**, 167 (2000).
[24] Ch. Skokos, J. Phys. A **34**, 10029 (2001).
[25] G. Contopoulos, *Order and Chaos in Dynamical Astronomy* (Springer-Verlag, Berlin, 2002).
[26] M. D. Hartl and A. Buonanno, Phys. Rev. D **71**, 024027 (2005).
[27] R. D. Ruth, IEEE Trans. Nucl. Sci. **30**, 2669 (1983).
[28] K. Feng, J. Comput. Math. **44**, 279 (1986).
[29] J. Wisdom and M. Holman, Astron. J. **102**, 1528 (1991).
[30] J. Xu and X. Wu, Res. Astron. Astrophys. **10**, 173 (2010).
[31] T. Y. Huang and K. Innanen, Astron. J. **88**, 870 (1983).
[32] V. A. Avdyushev, Celest. Mech. Dyn. Astron. **87**, 383 (2003).
[33] J. Baumgarte, Celest. Mech. **5**, 490 (1972).
[34] P. E. Nacozy, Astrophys. Space Sci. **14**, 40 (1971).
[35] M. A. Murrson, Astron. J. **97**, 1496 (1989).
[36] E. Hairer, C. Lubich, and G. Wanner, *Geometric Numerical Integration* (Springer, Berlin, 1999).
[37] H. Chin, Ph. D. thesis, University of British Columbia, 1995.
[38] U. M. Ascher, Numerical Algorithms **14**, 1 (1997).
[39] X. Wu, J. F. Zhu, J. Z. He, and H. Zhang, Comput. Phys. Commun. **175**, 15 (2006).
[40] X. Wu and J. Z. He, Int. J. Mod. Phys. C **17**, 1613 (2006).
[41] X. Wu, T. Y. Huang, X. S. Wan, and H. Zhang, Astron. J. **133**, 2643 (2007).
[42] V. Szebehely and D. G. Bettis, Astrophys. Space Sci. **13**, 365 (1971).
[43] L. Liu and X. H. Liao, Celest. Mech. Dyn. Astron. **59**, 221 (1994).
[44] T. Fukushima, Astron. J. **126**, 1097 (2003).
[45] D. Z. Ma, X. Wu, and J. F. Zhu, New Astronomy **13**, 216 (2008).
[46] T. Fukushima, Astron. J. **126**, 2567 (2003).
[47] T. Fukushima, Astron. J. **127**, 3638 (2004).
[48] D. Z. Ma, X. Wu, and S. Y. Zhong, Astrophys. J. **687**, 1294 (2008).
[49] D. Z. Ma, X. Wu, and F. Y. Liu, Int. J. Mod. Phys. C **19**, 1411 (2008).
[50] S. Y. Zhong and X. Wu, Astrophys. Space Sci. **324**, 31 (2009).
[51] X. Wu and Y. Xie, Phys. Rev. D **81**, 084045 (2010).
[52] T. Fukushima, Astron. J. **126**, 3138 (2003).
[53] X. Wu, T. Y. Huang, and H. Zhang, Phys. Rev. D **74**, 083001 (2006).
[54] X. Wu and T. Y. Huang, Phys. Lett. A **313**, 77 (2003).
[55] X. Wu, Res. Astron. Astrophys. **10**, 211 (2010).
[56] J. F. Zhu, X. Wu, and D. Z. Ma, Chin. J. Astron. Astrophys. **7**, 601 (2007).
[57] W. B. Han, Gen. Relativ. Gravit. **40**, 1831 (2008).
[58] N. J. Cornish and J. Levin, Phys. Rev. Lett. **89**, 179001 (2002).